

Manipulating vortices in F =2 Bose-Einstein condensates through magnetic field and spin-orbit coupling

Hao Zhu(朱浩), Shou-Gen Yin(印寿根), and Wu-Ming Liu(刘伍明)
Citation: Chin. Phys. B, 2022, 31 (**4**): 040306. DOI: 10.1088/1674-1056/ac398f
Journal homepage: http://cpb.iphy.ac.cn; http://iopscience.iop.org/cpb

What follows is a list of articles you may be interested in

Adjustable half-skyrmion chains induced by SU(3) spin-orbit coupling in rotating Bose-Einstein condensates

Li Wang(王力), Ji Li(李吉), Xiao-Lin Zhou(周晓林), Xiang-Rong Chen(陈向荣), and Wu-Ming Liu(刘伍明)
Chin. Phys. B, 2021, 30 (**11**): 110312. DOI: 10.1088/1674-1056/abfcc8

Spin-orbit-coupled spin-1 Bose-Einstein condensates confined in radially periodic potential

Ji Li(李吉), Tianchen He(何天琛), Jing Bai(白晶), Bin Liu(刘斌), and Huan-Yu Wang(王寰宇)
Chin. Phys. B, 2021, 30 (**3**): 030302. DOI: 10.1088/1674-1056/abc53e

Lattice configurations in spin-1 Bose–Einstein condensates with the SU(3) spin–orbit coupling

Ji-Guo Wang(王继国)†, Yue-Qing Li(李月晴), and Yu-Fei Dong(董雨菲)
Chin. Phys. B, 2020, 29 (**10**): 100304. DOI: 10.1088/1674-1056/abab72

Interference properties of two-component matter wave solitons

Yan-Hong Qin(秦艳红), Yong Wu(伍勇), Li-Chen Zhao(赵立臣), Zhan-Ying Yang(杨战营)
Chin. Phys. B, 2020, 29 (**2**): 020303. DOI: 10.1088/1674-1056/ab65b7

Periodically modulated interaction effect on transport of Bose-Einstein condensates in lattice with local defects

Kun-Qiang Zhu(朱坤强), Zi-Fa Yu(鱼自发), Ji-Ming Gao(高吉明), Ai-Xia Zhang(张爱霞), Hong-Ping Xu(徐红萍), Ju-Kui Xue(薛具奎)
Chin. Phys. B, 2019, 28 (**1**): 010307. DOI: 10.1088/1674-1056/28/1/010307

Manipulating vortices in $F = 2$ Bose–Einstein condensates through magnetic field and spin–orbit coupling

Hao Zhu(朱浩)[1], Shou-Gen Yin(印寿根)[1,†], and Wu-Ming Liu(刘伍明)[2,3,4,‡]

[1] *Key Laboratory of Display Materials and Photoelectric Devices (Ministry of Education), Tianjin Key Laboratory for Photoelectric Materials and Devices, School of Materials Science and Engineering, Tianjin University of Technology, Tianjin* 300384, *China*

[2] *Beijing National Laboratory for Condensed Matter Physics, Institute of Physics, Chinese Academy of Sciences, Beijing* 100190, *China*

[3] *School of Physical Sciences, University of Chinese Academy of Sciences, Beijing* 100190, *China*

[4] *Songshan Lake Materials Laboratory, Dongguan* 523808, *China*

(Received 20 October 2021; revised manuscript received 11 November 2021; accepted manuscript online 15 November 2021)

We investigate the vortex structures excited by Ioffe–Pritchard magnetic field and Dresselhaus-type spin–orbit coupling in $F = 2$ ferromagnetic Bose–Einstein condensates. In the weakly interatomic interacting regime, an external magnetic field can generate a polar-core vortex in which the canonical particle current is zero. With the combined effect of spin–orbit coupling and magnetic field, the ground state experiences a transition from polar-core vortex to Mermin–Ho vortex, in which the canonical particle current is anticlockwise. For fixed spin–orbit coupling strengths, the evolution of phase winding, magnetization, and degree of phase separation with magnetic field are studied. Additionally, with further increasing spin–orbit coupling strength, the condensate exhibits symmetrical density domains separated by radial vortex arrays. Our work paves the way to explore exotic topological excitations in high-spin systems.

Keywords: Bose–Einstein condensates, vortex, magnetic field, spin–orbit coupling

PACS: 03.75.Lm, 03.75.Hh, 03.75.Nt, 05.30.Jp **DOI:** 10.1088/1674-1056/ac398f

1. Introduction

Vortex is one of the most fundamental topological excitations appearing in various fields of modern physics.[1–3] In scalar Bose–Einstein condensates (BECs), the quantized vortex was firstly realized by Ketterle's group[4] which plays a significant role in systematically studying superfluidity and superconductivity.[5–7] Various novel topological nontrivial structures in spinor BECs have been realized, *i.e.*, vortex-bright soliton,[8] 8π skyrmion,[9] and carbon-dioxide-like skyrmion.[10] There are many methods for generating vortices in real experiments, including phase imprinting techniques,[11] rotating an anisotropic trap,[12] or stirring the condensate with laser beams.[13] However, with the effort of artificial gauge field in cold atom experiments, Spielman's group generated vortices by laser control techniques,[14–16] which opens a new gate in manipulating topological excitations from spinor BECs.

Artificial spin–orbit coupling (SOC) induced by synthetic gauge fields is a newly developing technique in ultracold physics, which can be equivalently depicted as the interaction between an effective non-Abelian gauge potential and a particle with spin freedom.[17–19] The spin–orbit (SO) effect has attracted much attention from different researchers, and the topological nontrivial vortices in spinor BEC systems are systematically investigated.[20–22] To realize vortex or vortex lattice in SO coupled BEC system through external rotation, not only harmonic trap, but also Raman laser beams require being rotated,[23] that is difficult to realize in real experiments. In the present case, the method of Raman laser dressing reflects its advantage,[24] because the lasers are stationary and the trapping potential is time-independent in the laboratory frame. Accompanying by the appearance of SOC, the mechanical angular momentum $L_z^{\rm mech} = L_z^{\rm c} + L_z^{\rm s}$ with canonical angular momentum $L_z^{\rm c} = (\boldsymbol{r} \times \boldsymbol{p})_z$ and gauge angular momentum $L_z^{\rm s} = -(\boldsymbol{r} \times \boldsymbol{A})_z$.[25–27] Actually, instead of directly introducing canonical angular momentum by rotation, SOC can introduce gauge angular momentum which could also generate vortex structures.[28–31] The aforementioned method avoid the shortcoming of rotating the condensate in SO coupled system.

In this paper, we apply Dresselhaus-type SOC in the $F = 2$ ferromagnetic BECs under additional Ioffe–Pritchard (IP) magnetic field to generate vortex structures. When SOC is absent, polar-core vortex is excited by magnetic field. When considering SOC, Mermin–Ho vortex is introduced to the system. Moreover, canonical particle currents of polar-core vortex and Mermin–Ho vortex are studied. Through calculating phase winding, magnetization, and degree of phase separation, the evolution of the vortex is discussed when magnetic field is changed. On the other hand, the influence of SOC on the vortex is investigated.

This paper is organized as follows: We first introduce the model Hamiltonian in Section 2. The mean-field ground states

†Corresponding author. E-mail: sgyin@tjut.edu.cn

‡Corresponding author. E-mail: wmliu@iphy.ac.cn

© 2022 Chinese Physical Society and IOP Publishing Ltd

of $F=2$ BECs with IP magnetic field are studied by numerically minimizing the Hamiltonian function, and the polar-core vortex is discussed in Subsection 3.1. The mean-field ground states of $F=2$ BECs with IP magnetic field and SOC are investigated, Mermin–Ho vortex and vortex lattice are discussed in Subsection 3.2. Eventually, Section 4 is devoted to concluding remarks.

2. Model Hamiltonian

We consider a two-dimensional (2D) $F=2$ BECs with Dresselhaus-type SOC and external IP magnetic field. The mean-field Hamiltonian can be depicted as[32–34]

$$\begin{aligned}\mathcal{H} =& \int \mathrm{d}\boldsymbol{r}\boldsymbol{\Psi}^{\dagger}\left(-\frac{\hbar^2}{2m}\nabla^2+\mathcal{V}_{\mathrm{H}}+\mathcal{V}_{\mathrm{SO}}+\mu_{\mathrm{B}}g_{\mathrm{F}}\boldsymbol{B}\cdot\boldsymbol{F}\right)\boldsymbol{\Psi}\\&+\int \mathrm{d}\boldsymbol{r}\left(\frac{c_0}{2}\boldsymbol{\rho}^2+\frac{c_1}{2}|\boldsymbol{F}|^2+\frac{c_2}{2}|\boldsymbol{\Theta}|^2\right),\end{aligned}\tag{1}$$

where $\boldsymbol{\Psi}=[\Psi_2(\boldsymbol{r}),\Psi_1(\boldsymbol{r}),\Psi_0(\boldsymbol{r}),\Psi_{-1}(\boldsymbol{r}),\Psi_{-2}(\boldsymbol{r})]$ characterizes the macroscopic wave function of the condensate, m is the atomic mass, and $n=\sum_l n_l=\sum_l|\Psi_l|^2$ is the total particle density, where $l=\pm2,\pm1,0$. The two-dimensional (2D) wave functions are normalized as $\int n\mathrm{d}x\mathrm{d}y=N$. The harmonic potential is $\mathcal{V}_{\mathrm{H}}=(1/2)m\omega_{\perp}^2(x^2+y^2)$ with $\omega_{\perp}$ characterizing the harmonic frequency in x and y directions, μ_{B} is Bohr magneton, and $g_{\mathrm{F}}=-1/2$ is the Landé g_{F} factor. The strengths of density–density interaction, spin-exchange interaction, and spin singlet-pairing interaction are $c_0=2\hbar^2(4a_2+3a_4)/(7m)$, $c_1=2\hbar^2(a_4-a_2)/(7m)$, and $c_2=2\hbar^2(7a_0-10a_2+3a_4)/(7m)$, where a_0, a_2, and a_4 represent the s-wave scattering lengths in total spin $f_{\mathrm{tot}}=0$, 2, and 4 channels.[35] $\boldsymbol{F}=(F_x,F_y,F_z)=(\boldsymbol{\Psi}^{\dagger}\hat{F}_x\boldsymbol{\Psi},\boldsymbol{\Psi}^{\dagger}\hat{F}_y\boldsymbol{\Psi},\boldsymbol{\Psi}^{\dagger}\hat{F}_z\boldsymbol{\Psi})$ with spin-2 matrices $\hat{F}_{x,y,z}$, $\boldsymbol{\Theta}=c_2(2\psi_2\psi_{-2}-\psi_1\psi_{-1}+\psi_0^2)/5$ is the amplitude of spin singlet-pair. The Dresselhaus-type SOC term can be characterized as $\mathcal{V}_{\mathrm{SO}}=-\mathrm{i}\hbar\kappa(F_y\partial_x+F_x\partial_y)$, where κ is the SOC strength. The external IP magnetic field is depicted as: $\boldsymbol{B}(\boldsymbol{r})=B(x\hat{x}-y\hat{y})$, where B is the radial field gradient in the x–y plane, and $\hat{x},\hat{y}$ are unit vectors along the x,y directions, respectively.[36] For numerical calculations, it is convenient to make the following parameter transformations:

$$\begin{aligned}&x=\xi_0\tilde{x},\quad y=\xi_0\tilde{y},\quad t=\omega_{\perp}^{-1}\tilde{t},\\&\kappa=\omega_{\perp}\xi_0\tilde{\kappa},\quad B=\hbar\omega_{\perp}/(\mu_{\mathrm{B}}g_{\mathrm{F}}\xi_0)\tilde{B},\\&\Psi_l=\sqrt{N}\xi_0^{-1}\tilde{\Psi}_l,\quad c_{0,1,2}=4\pi N\tilde{c}_{0,1,2},\end{aligned}\tag{2}$$

where the length of the trap unit is $\xi_0=\sqrt{\hbar/m\omega_{\perp}}$. In the mean-field approximation, the $F=2$ BECs can be described by the following dimensionless Gross–Pitaevskii (GP) equations:[32–34]

$$\begin{aligned}\mathrm{i}\frac{\partial\tilde{\Psi}_{\pm2}}{\partial\tilde{t}} =& \left[-\frac{1}{2}\tilde{\nabla}^2+\tilde{V}_{\mathrm{ext}}+\tilde{c}_0\tilde{n}\right]\tilde{\Psi}_{\pm2}+\frac{\tilde{c}_2}{\sqrt{5}}\tilde{\Theta}\tilde{\Psi}_{\mp2}^{\dagger}\\&+\tilde{c}_1\left(\tilde{F}_{\mp}\tilde{\Psi}_{\pm1}\pm2\tilde{F}_z\tilde{\Psi}_{\pm2}\right)+\tilde{\kappa}(\mp\partial_x-\mathrm{i}\partial_y)\Psi_{\pm1}\\&+\mathrm{i}\tilde{B}(\tilde{x}\pm\mathrm{i}\tilde{y})\tilde{\Psi}_{\pm1},\end{aligned}\tag{3}$$

$$\begin{aligned}\mathrm{i}\frac{\partial\tilde{\Psi}_{\pm1}}{\partial\tilde{t}} =& \left[-\frac{1}{2}\tilde{\nabla}^2+\tilde{V}_{\mathrm{ext}}+\tilde{c}_0\tilde{n}\right]\tilde{\Psi}_{\pm1}-\frac{\tilde{c}_2}{\sqrt{5}}\tilde{\Theta}\tilde{\Psi}_{\mp1}^{\dagger}\\&+\tilde{c}_1\left(\frac{\sqrt{6}}{2}\tilde{F}_{\mp}\tilde{\Psi}_0+\tilde{F}_{\pm}\tilde{\Psi}_{\pm2}\pm\tilde{F}_z\tilde{\Psi}_{\pm1}\right)\\&+\tilde{\kappa}(\pm\partial_x-\mathrm{i}\partial_y)\Psi_{\pm2}+\frac{\sqrt{6}}{2}\tilde{\kappa}(\mp\partial_x-\mathrm{i}\partial_y)\Psi_0\\&+\mathrm{i}\tilde{B}(\tilde{x}\mp\mathrm{i}\tilde{y})\tilde{\Psi}_{\pm2}+\frac{\sqrt{6}}{2}\mathrm{i}\tilde{B}(\tilde{x}\pm\mathrm{i}\tilde{y})\tilde{\Psi}_0,\end{aligned}\tag{4}$$

$$\begin{aligned}\mathrm{i}\frac{\partial\tilde{\Psi}_0}{\partial\tilde{t}} =& \left[-\frac{1}{2}\tilde{\nabla}^2+\tilde{V}_{\mathrm{ext}}+\tilde{c}_0\tilde{n}\right]\tilde{\Psi}_0+\frac{\tilde{c}_2}{\sqrt{5}}\tilde{\Theta}\tilde{\Psi}_0^{\dagger}\\&+\frac{\sqrt{6}}{2}\tilde{c}_1\left(\tilde{F}_-\tilde{\Psi}_{-1}+\tilde{F}_+\tilde{\Psi}_1\right)+\frac{\sqrt{6}}{2}\tilde{\kappa}(\partial_x-\mathrm{i}\partial_y)\Psi_1\\&+\frac{\sqrt{6}}{2}\tilde{\kappa}(-\partial_x-\mathrm{i}\partial_y)\Psi_{-1}+\frac{\sqrt{6}}{2}\mathrm{i}\tilde{B}(\tilde{x}\mp\mathrm{i}\tilde{y})\tilde{\Psi}_{\pm1},\end{aligned}\tag{5}$$

where $\tilde{F}_z=2\left(|\tilde{\Psi}_2|^2-|\tilde{\Psi}_{-2}|^2\right)+|\tilde{\Psi}_1|^2-|\tilde{\Psi}_{-1}|^2$, $\tilde{F}_+=\tilde{F}_-^{\dagger}=2\left(\tilde{\Psi}_2^{\dagger}\tilde{\Psi}_1+\tilde{\Psi}_{-1}^{\dagger}\tilde{\Psi}_{-2}\right)+\sqrt{6}\left(\tilde{\Psi}_1^{\dagger}\tilde{\Psi}_0+\tilde{\Psi}_0^{\dagger}\tilde{\Psi}_{-1}\right)$, and $\tilde{V}_{\mathrm{ext}}=(1/2)\left(\tilde{x}^2+\tilde{y}^2\right)$. For simplicity, it will be convenient to drop off the tilde in the following calculation.

In order to thoroughly investigate the properties of the vortex solution, the coupled GP equations (3)–(5) are solved by Crank–Nicolson method.[37] We have verified the stationary state solutions by starting the calculation from a variety of initial conditions, such as the Gaussian-like functions. The density–density interaction $c_0=50$, the spin-exchange interaction $c_1=-5$, and the spin singlet-pairing $c_2=20$ are fixed throughout the whole calculation.

3. Results and discussion

3.1. Ground states with IP magnetic field

We first investigate the vortex solution in the weak interatomic interacting region, where the density–density interaction $c_0=50$, spin-exchange interaction $c_1=-5$, and spin singlet-pairing interaction $c_2=20$ guarantee the ferromagnetic ground states.[38] When SOC is absent, the weak magnetic field ($B=0.1$) can induce a vortex at the edge of the condensate, which is depicted in Fig. 1(a). As indicated by the 2D density profiles of different components ($|\Psi_l|^2$) in the top panel, there is no vortex core emerging. However, from the phase field picture in the bottom panel, the continuously changed phase gradients θ_l (from $-\pi$ to π) indicate there is a vortex penetrating into the condensate from the edge. The corresponding one-dimensional (1D) density projection is exhibited in Fig. 1(b), that there are five Gaussian-type wave packages locating at the center. Additionally, when magnetic field strength $B=1$, a polar-core vortex is excited in Fig. 1(c).[39–41] The 2D density profiles (top

panel) indicate the ring-shaped density of different components with a vortex core in the center. This polar-core vortex can be determined clearly from the phase profiles (bottom panel), that the phase windings of different components are $(\omega_2,\omega_1,\omega_0,\omega_{-1},\omega_{-2})=(2,1,0,-1,-2)$. The corresponding 1D density projection is exhibited in Fig. 1(d), that the components with opposite magnetic quantum number ($|\Psi_2\rangle$ and $|\Psi_{-2}\rangle$, $|\Psi_1\rangle$, and $|\Psi_{-1}\rangle$) are totally overlapped.

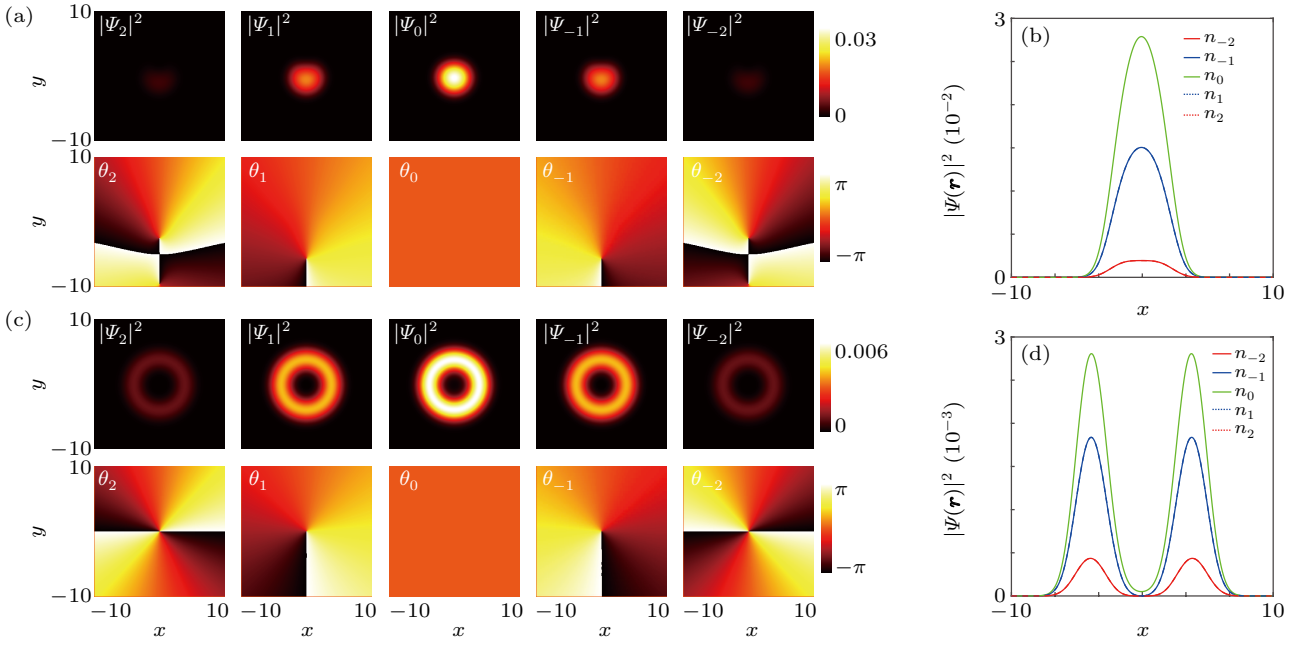


Fig. 1. Magnetic field could induce polar-core vortex when SOC is absent. (a) The 2D density profiles of different components when magnetic field strength $B=0.1$ and SOC strength $\kappa=0$ (top panel). The corresponding phase fields θ_l ($l=\pm2,\pm1,0$) are exhibited in the bottom panel. (b) The 1D projection of the density profiles with $B=0.1$ and $\kappa=0$. (c) The 2D density profiles of different components when magnetic field strength $B=1$ and SOC strength $\kappa=0$ (top panel). The corresponding phase fields θ_l are exhibited in the bottom panel. (d) The 1D projection of the density profiles with $B=1$ and $\kappa=0$. In the GP simulation, the dimensionless density–density interaction $c_0=50$, spin-exchange interaction $c_1=-5$, and spin singlet-pairing $c_2=20$. Here, the length of the harmonic trap is $\xi_0=\sqrt{\hbar/(m\omega_\perp)}$.

3.2. Ground states with IP magnetic field and SOC

In the following part, we will consider the combined effect of IP magnetic field and Dresselhaus-type SOC in the weak atomic interaction region of ferromagnetic $F=2$ BECs. When magnetic field $B=0.25$ and SOC strength $\kappa=0.25$, the 2D density profiles and phase fields are depicted in the top panel and bottom panel of Fig. 2(a), respectively. The $|\Psi_2\rangle$ component dominates the center region and resembles bright soliton. Additionally, the $|\Psi_{1,0,-1,-2}\rangle$ components exhibit ring-shaped distribution with increasing inner diameter. From the phase field in the bottom panel, we can distinguish that the phase windings of different components are $(\omega_2,\omega_1,\omega_0,\omega_{-1},\omega_{-2})=(0,-1,-2,-3,-4)$, which indicates a Mermin–Ho vortex.[42–44] From the 1D density projection in Fig. 2(b) we can identify that the $|\Psi_2\rangle$ component locates in the center, the $|\Psi_{-2}\rangle$ component locates at the edge and $|\Psi_{1,0,-1}\rangle$ components locate sandwiched between them. When SOC strength $\kappa=1$ and IP magnetic field strength $B=0.25$, there is a density hole emerging in every component, as shown in the top panel of Fig. 2(c). Interestingly, the corresponding phase windings can be distinguished from the phase field in the bottom panel that $(\omega_2,\omega_1,\omega_0,\omega_{-1},\omega_{-2})=(-1,-2,-3,-4,-5)$. Moreover, figure 2(d) shows that the different components with opposite magnetic quantum number ($|\Psi_2\rangle$ and $|\Psi_{-2}\rangle$, $|\Psi_1\rangle$ and $|\Psi_{-1}\rangle$) are spatially separated which indicates nonzero magnetization.

We can gain further insight into the discussed vortex solution by computing the canonical particle current density of the condensates[45]

$$J^{\mathrm{c}}=\sum_l J_l^{\mathrm{c}}=-\frac{\mathrm{i}\hbar}{2m}\sum_l(\Psi_l^{\dagger}\nabla\Psi_l-\Psi_l\nabla\Psi_l^{\dagger}), \tag{6}$$

where $l=\pm2,\pm1,0$ and m represents the atom mass. As illustrated in Fig. 3(a), when SOC is absent and magnetic field $B=0.1$, the canonical particle current J^{c} points toward $+y$ direction, indicating the condensates are within the plane wave phase.[31] Furthermore, with stronger magnetic field ($B=0.25$) in Fig. 3(b), the canonical particle current J^{c} approximates zero. This phenomenon is in good agreement with the phase field of the polar-core vortex shown in Fig. 1(c) that $\theta_{-1,-2}$ rotate anticlockwise while $\theta_{1,2}$ rotate clockwise. On the other hand, when SOC strength $\kappa=1$ and magnetic field $B=0.25$ in Fig. 3(c), the canonical particle current J^{c} rotates anticlockwise. This phenomenon coincides with the MH vortex discussed in Fig. 2(a), inside which $\theta_{-1,0,1,2}$ rotate anticlockwise. Moreover, with the strengthen of magnetic field ($\kappa=1$) in Fig. 3(d), the direction of canonical particle current J^{c} remains anticlockwise while the size of vortex core becomes larger.

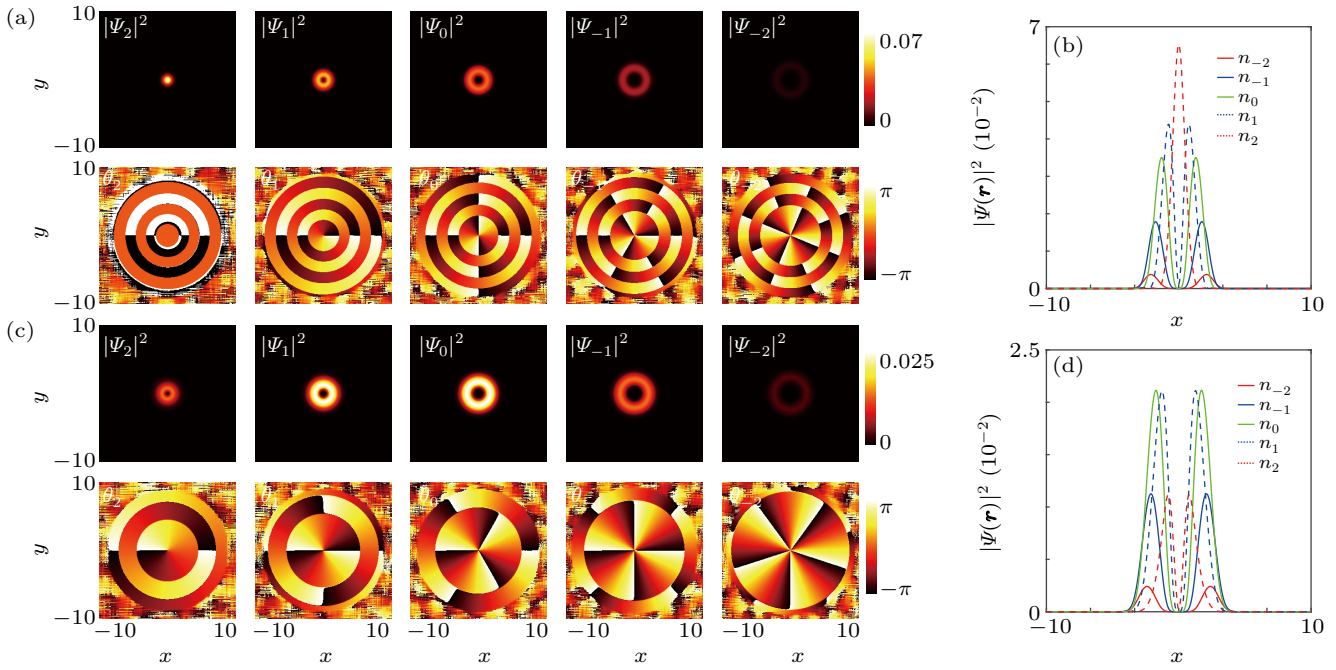


Fig. 2. The combined effect of magnetic field and SOC-induced Mermin–Ho vortex. (a) The 2D density profiles of different components when magnetic field strength $B = 0.25$ and SOC strength $\kappa = 0.25$ (top panel). The corresponding phase fields θ_l ($l = \pm 2, \pm 1, 0$) are exhibited in the bottom panel. (b) The 1D projection of the density profiles when $B = 0.25$ and $\kappa = 0.25$. (c) The 2D density profiles of different components when magnetic field strength $B = 0.25$ and SOC strength $\kappa = 1$ (top panel). The corresponding phase fields θ_l are exhibited in the bottom panel. (d) The 1D projection of the density profiles when $B = 0.25$ and $\kappa = 1$. In the GP simulation, the dimensionless density–density interaction $c_0 = 50$, spin-exchange interaction $c_1 = -5$, and spin-singlet-pairing interaction $c_2 = 20$. Here, the length of the harmonic trap is $\xi_0 = \sqrt{\hbar/(m\omega_\perp)}$.

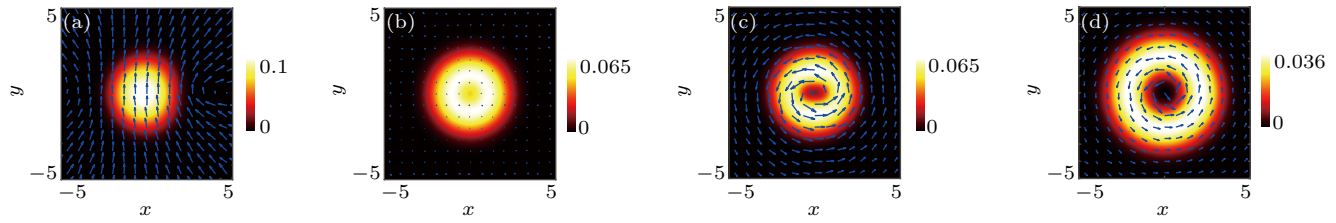


Fig. 3. Canonical particle current J^c induced by IP magnetic field B and SOC κ. (a) Total density and J^c with $B = 0.1$, $\kappa = 0$. (b) Total density and J^c with $B = 0.25$, $\kappa = 0$. (c) Total density and J^c with $B = 0.25$, $\kappa = 0.25$. (d) Total density and J^c with $B = 0.25$, $\kappa = 1$. The blue arrows indicate the direction of canonical particle current. In the GP simulation, the dimensionless density–density interaction $c_0 = 50$, spin-exchange interaction $c_1 = -5$, and spin-singlet-pairing interaction $c_2 = 20$. Here, the length of the harmonic trap is $\xi_0 = \sqrt{\hbar/(m\omega_\perp)}$.

For fixing SOC strengths, we next investigate the evolution of phase winding when IP magnetic field strength B is changed. As depicted in Fig. 4(a) that SOC is absent in the system, the phase windings for different components maintain their value $(\omega_2, \omega_1, \omega_0, \omega_{-1}, \omega_{-2}) = (2, 1, 0, -1, -2)$ when B varies in [0.25,2] region. Apparently, the aforementioned polar-core vortex is not influenced by IP magnetic field when SOC is absent. As comparison in Fig. 4(b) that SOC strength $\kappa = 1$, the phase windings experience a transformation $(\omega_2, \omega_1, \omega_0, \omega_{-1}, \omega_{-2})$:

$$\begin{aligned}&(0,-1,-2,-3,-4) \to (-1,-2,-3,-4,-5)\\ &\to (-3,-4,-5,-6,-7) \to (-4,-5,-6,-7,-8)\\ &\to (-5,-6,-7,-8,-9)\end{aligned}$$

when B varies in [0.25,2] region. This phenomenon can be understood that the SOC induced gauge angular momentum can introduce negative canonical angular momentum, which results in a vortex with winding number $(-2,-2,-2,-2,-2)$. Correspondingly, the polar-core vortex with phase winding $(2,1,0,-1,-2)$ changes into the MH vortex with phase winding $(0,-1,-2,-3,-4)$. Furthermore, giant vortices with greater phase winding number combinations are formed because of stronger IP magnetic field strength.

The magnetization of $F = 2$ BECs ground states can be defined as $\mathcal{M} = \int F_z \mathrm{d}x\mathrm{d}y$, where F_z is the z-direction spin density of the five-component systems.[46] Depending on various IP magnetic field, the evolution of $\mathcal{M}$ is investigated in Figs. 4(c) and 4(d). When SOC is absent, the magnetization of the ground state keeps zero for different magnetic fields which agrees well with the superposition of the different components with opposite magnetic quantum number, as shown in Fig. 4(c). However, when SOC strength $\kappa = 1$, the magnetization reaches maximum at $B = 0.5$ and decreases monotonously for $B > 0.5$.

On the other hand, we are also interested in the misibility of the condensate when IP magnetic field is changed.

We defined the degree of phase separation as $n_{\rm p} = \int |F_z| {\rm d}r$, where F_z is the z-direction spin density of the five-component system.[47] For SOC strength $\kappa = 0$ in Fig. 4(e), the degree of phase separation is not influenced by IP magnetic field ($n_{\rm p} = 0$). This phenomenon indicates that without SOC, the condensate is totally miscible when facing IP magnetic field. However, $n_{\rm p}$ can be obviously changed by IP field when SOC effect is considered, as shown in Fig. 4(f). The degree of phase separation $n_{\rm p}$ increases with magnetic field when $B < 0.5$, while decreases with magnetic field when $B > 0.5$.

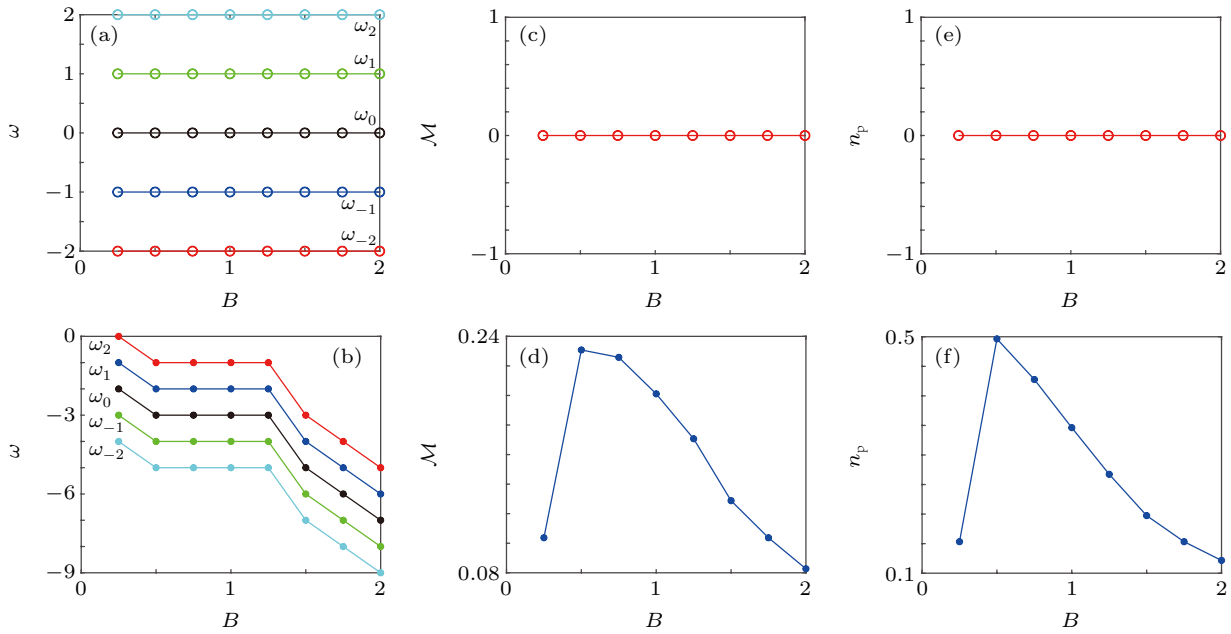


Fig. 4. Phase windings of different components vary as a function of magnetic field strength B without SOC in panel (a) and with SOC $\kappa = 1$ in panel (b). Magnetization $\mathcal{M} = \int F_z {\rm d}x{\rm d}y$ varies with B without SOC in panel (c) and with SOC in panel (d). Degree of phase separation $n_{\rm p} = \int |F_z| {\rm d}r$ varies with B without SOC in panel (e) and with SOC $\kappa = 1$ in panel (f). In the GP simulation, the dimensionless density–density interaction $c_0 = 50$, spin-exchange interaction $c_1 = -5$, and spin-singlet-pairing interaction $c_2 = 20$. Here, the length of the harmonic trap is $\xi_0 = \sqrt{\hbar/(m\omega_\perp)}$.

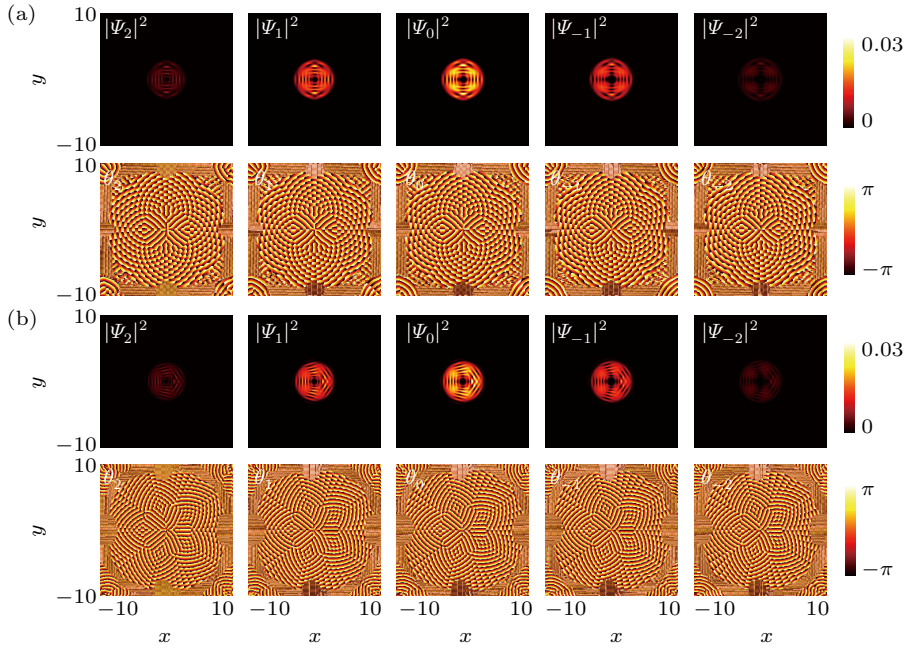


Fig. 5. Density distribution (top panel) and phase field (bottom panel) of different components as a function of SOC. The symmetrical density domains separated by vortex arrays with magnetic field strength $B = 1$ and $\kappa = 4.5$ in panel (a), $\kappa = 6$ in panel (b). In the GP simulation, the dimensionless density–density interaction $c_0 = 50$, spin-exchange interaction $c_1 = -5$, and spin-singlet-pairing interaction $c_2 = 20$. Here, the length of the harmonic trap is $\xi_0 = \sqrt{\hbar/(m\omega_\perp)}$.

At last, we investigate the evolution of vortex for various SOC strength when IP magnetic field is fixed ($B = 1$). Along with the SOC strength κ increasing, additional vortices are generated and align radially, as depicted in Figs. 5(a)–5(b) with $\kappa = 4.5, 6$, respectively. These vortices act as domain walls that separate the condensates into four and five symmet-

rical density domains. We notice that the vortex structures in different components resemble each other. It is found that the number of vortices in each array is equal and increases with SOC strength κ. The vortices in every component share the same winding number $\omega_l = -1$, except for the central giant vortex, the internal diameter of which is bigger for stronger SOC strength.

4. Conclusion

In summary, we have investigated the ground state vortex solution under the IP magnetic field and Dresselaus-type SOC in $F = 2$ BECs. When SOC is absent, polar-core vortex is obtained which is not influenced for stronger magnetic field. When considering SOC, MH vortex is excited with the combined effect of the magnetic field. By calculating the canonical particle current, we can identify zero canonical particle current of polar-core vortex and anticlockwise canonical particle current of MH vortex. When SOC strength is fixed, the evolution of phase winding, magnetization and degree of phase separation are thoroughly investigated. On the other hand, when magnetic field is fixed, stronger SOC may introduce additional vortices which are arranged radially acting as domain walls.

Acknowledgments

Project supported by the National Key Research and Development Program of China (Grant No. 2016YFA0301500), the National Natural Science Foundation of China (Grant Nos. 61835013 and 11971067), the Strategic Priority Research Program of the Chinese Academy of Sciences (Grant Nos. XDB01020300 and XDB21030300), Beijing Natural Science Foundation, China (Grant No. 1182009), and Beijing Great Wall Talents Cultivation Program, China (Grant No. CIT&TCD20180325).

References

[1] Goldstein L 1953 *Phys. Rev.* **89** 597
[2] Pincus P and Shapiro K A 1965 *Phys. Rev. Lett.* **15** 597
[3] Fetter A L 1971 *Phys. Rev. Lett.* **27** 986
[4] Abo-Shaeer J R, Raman C, Vogels J M and Ketterle W 2001 *Science* **292** 5516
[5] Babaev E 2008 *Phys. Rev. B* **77** 054512
[6] Tserkovnyak Y and Zou J 2019 *Phys. Rev. Research* **1** 033071
[7] Uji S, Terashima T, Terai Y, Yasuzuka S, Tokumoto M, Tanaka H, Kobayashi A and Kobayashi H 2005 *Phys. Rev. B* **71** 104525
[8] Law K J H, Kevrekidis P G and Tuckerman L S 2010 *Phys. Rev. Lett.* **105** 160405
[9] Mueller E J 2003 *Phys. Rev. A* **69** 033606
[10] Liu C F, Juzeliūnas G and Liu W M 2016 *Phys. Rev. A* **95** 023624
[11] Williams J E and Holland M J 1999 *Nature* **401** 568
[12] McEndoo S and Busch T 2010 *Phys. Rev. A* **82** 013628
[13] Madison K W, Chevy F, Wohlleben W and Dalibard J 2000 *Phys. Rev. Lett.* **84** 806
[14] Lin Y J, Compton R L, Jiménez-García K, Porto J V and Spielman I B 2009 *Nature* **462** 628
[15] Spielman I B 2009 *Phys. Rev. A* **79** 063613
[16] LeBlanc L J, Jiménez-García K, Williams R A, Beeler M C, Phillips W D and Spielman I B 2015 *New J. Phys.* **17** 065016
[17] Cooper N R, Dalibard J and Spielman I B 2018 *Rev. Mod. Phys.* **91** 015005
[18] Zhang Y, Mao L and Zhang C 2011 *Phys. Rev. Lett.* **108** 035302
[19] Sinha S, Nath R and Santos L 2011 *Phys. Rev. Lett.* **107** 270401
[20] Jian C M and Zhai H 2011 *Phys. Rev. B* **84** 060508(R)
[21] Kawakami T, Mizushima T and Machida K 2011 *Phys. Rev. A* **84** 011607(R)
[22] Ramachandhran B, Opanchuk B, Liu X J, Pu H, Drummond P D and Hu H 2012 *Phys. Rev. A* **85** 023606
[23] Fetter A L 2013 *Phys. Rev. A* **89** 023629
[24] Radić J, Sedrakyan T A, Spielman I B and Galitski V 2011 *Phys. Rev. A* **84** 063604
[25] Stringari S 2016 *Phys. Rev. Lett.* **118** 145302
[26] Zhou X F, Zhou J and Wu C 2011 *Phys. Rev. A* **84** 063624
[27] Qu C and Stringari S 2018 *Phys. Rev. Lett.* **120** 183202
[28] Jin J, Han W and Zhang S 2018 *Phys. Rev. A* **98** 063607
[29] Ruokokoski E, Huhtamäki, J A M and Möttönen M 2012 *Phys. Rev. A* **86** 051607(R)
[30] Zhou X F, Zhou Z W, Wu C J and Guo G C 2015 *Phys. Rev. A* **91** 033603
[31] Wang C, Gao C, Jian C M and Zhai H 2010 *Phys. Rev. Lett.* **105** 160403
[32] Xu Z F, Kawaguchi Y, You L and Ueda M 2012 *Phys. Rev. A* **86** 033628
[33] Saito H and Ueda M 2005 *Phys. Rev. A* **72** 053628
[34] Ueda M and Koashi M 2002 *Phys. Rev. A* **65** 063602
[35] Widera A, Gerbier F, Fölling S, Gericke T, Mandel O and Bloch I 2006 *New J. Phys.* **8** 152
[36] Leanhardt A E, Görlitz A, Chikkatur A P, Kielpinski D, Shin Y, Pritchard D E and Ketterle W 2002 *Phys. Rev. Lett.* **89** 190403
[37] Leiler G and Rezzolla L 2006 *Phys. Rev. D* **73** 044001
[38] Gautam S and Adhikari S K 2015 *Phys. Rev. A* **91** 013624
[39] Bulgakov E N and Sadreev A F 2002 *Phys. Rev. Lett.* **90** 200401
[40] Sadler L E, Higbie J M, Leslie S R, Vengalattore M and Stamper-Kurn D M 2006 *Nature* **443** 312
[41] Kobayashi S, Kawaguchi Y, Nitta M and Ueda M 2012 *Phys. Rev. A* **86** 023612
[42] Mizushima T, Machida K and Kita T 2002 *Phys. Rev. Lett.* **89** 030401
[43] Mizushima T, Kobayashi N and Machida K 2004 *Phys. Rev. A* **70** 043613
[44] Martikainen J P, Collin A and Suominen K A 2002 *Phys. Rev. A* **66** 053604
[45] Kawaguchi Y and Ueda M 2012 *Phys. Rep.* **520** 253
[46] Gautam S and Adhikari S K 2015 *Phys. Rev. A* **91** 013624
[47] Xu X Q and Han H J 2011 *Phys. Rev. Lett.* **107** 200401